Computational Materials Science 183 (2020) 109843

Contents lists available at ScienceDirect

Computational Materials Science

journal homepage: www.elsevier.com/locate/commatsci

Tailoring the structural properties and electronic structure of anatase, brookite and rutile phase TiO_2 nanoparticles: DFTB calculations

Hasan Kurban[a,b], Mehmet Dalkilic[a], Selçuk Temiz[c], Mustafa Kurban[d,*]

[a] Computer Science Department, Indiana University, Bloomington 47405 IN, USA
[b] Computer Engineering Department, Siirt University, 56100 Siirt, Turkey
[c] Department of Metallurgical and Materials Engineering, Eskişehir Osmangazi University, 26040 Eskişehir, Turkey
[d] Department of Electronics and Automation, Kırşehir Ahi Evran University, 40100 Kırşehir, Turkey

ARTICLE INFO

Keywords:
Nanoparticles
TiO_2
Segregation phenomena
DFTB

ABSTRACT

In this study, we perform a theoretical investigation using the density functional tight-binding (DFTB) approach for the structural analysis and electronic structure of anatase, brookite and rutile phase TiO_2 nanoparticles (NPs). Our results show that the number of Ti-O bonds is greater than that of O-O, while the number of Ti-Ti bonds is fewer. Thus, large amounts of O atoms prefer to connect to Ti atoms. The increase in the temperature of the NPs contributes to an increase in the interaction of Ti–O bonding, but a decrease in the O-O bonding. The segregation of Ti and O atoms shows that Ti atoms tend to co-locate at the center, while O atoms tend to reside on the surface. Increasing temperature causes a decrease of the bandgap from 3.59 to 2.62 eV for the brookite phase, which is much more energetically favorable compared to the bulk, while it could increase the bandgap from 3.15 to 3.61 eV for anatase phase. For three-phase TiO_2 NPs, LUMO and Fermi levels decrease. The HOMO level of anatase phase NP decreases, but it increases for brookite and rutile phase TiO_2 nanoparticles. An increase in the temperature contributes to the stabilization of anatase phase TiO_2 NP due to a decrease in the HOMO energies.

1. Introduction

Titanium dioxide (TiO_2) has attracted intense scrutiny as a photocatalyst in water splitting pigments, gas sensors, in hydrogen gas evolution, self-cleaning surfaces, solar cells, *etc.,* [1] owing to its catalytic properties that provide good stability, non-toxicity, and low-cost production [2–6]. TiO_2 is known to naturally occur in mineral forms—the most abundant being rutile and as other rarer polymorphs anatase and brookite [7]. These various polymorphs exhibit different phase characteristics due to the deviation in the lattice arrangements that can be exploited for various applications. For example, anatase demonstrates the highest photocatalytic activity [8–10] compared to either brookite or rutile, whereas the photocatalytic activity of defective brookite is better than either anatase or rutile [11]. Observing the bandgap of bulk TiO_2 is 3.2, 3.1 and 3.0 eV for anatase, brookite and rutile, respectively [12–14], a large bandgap restricts its use, however, only to the narrow light-response range of ultraviolet (only about 3–5% of solar spectrum) [15]. The bandgap is significantly affected by factors like phase structure, temperature, and crystal size. TiO_2 nanoparticles (NPs) have recently been receiving more attention in organic synthesis [16–18], in different inorganic and organic reactions [19–22], and in the preparation of derivations of molecules [23–26], because of their useful and unique properties. Additionally, TiO_2 NPs are used in health and the environment *e.g.,* environmental remediation, self-cleaning and self-disinfection [27,28], and in novel biomedical applications [29,30]. There has also been prior work using DFTB on TiO_2 and TiN nanoparticles that have shown that these systems typically are intermixed with each other (i.e., TiO_2 readily mixes with TiN and vice versa) in realistic environments [31].

Improving the performance of NP materials can be achieved using different approaches, for example, by adding an atom, applying pressure, increasing the temperature, and modifying crystallite size that change their morphologies [32–35]. By applying this general principle, this work presents the structural and electronic properties of TiO_2 NPs by using the density functional based tight binding (DFTB) method to study the influence of the temperature on the three different phases, anatase, brookite and rutile of TiO_2 NPs. The performance of DFTB calculations has been shown on NPs in the previous studies [36,37]. In this study, we analyzed the HOMO, LUMO and the frontier molecular orbital energy gap (E_g), total energy, density of states (DOS), radial distribution functions (RDFs), order parameter (R) to analyze the segregation phenomena of Ti and O atoms and the number of bonds

* Corresponding author.
E-mail addresses: mkurbanphys@gmail.com, mkurban@ahievran.edu.tr (M. Kurban).

https://doi.org/10.1016/j.commatsci.2020.109843
Received 11 April 2020; Received in revised form 25 May 2020; Accepted 26 May 2020
Available online 31 May 2020

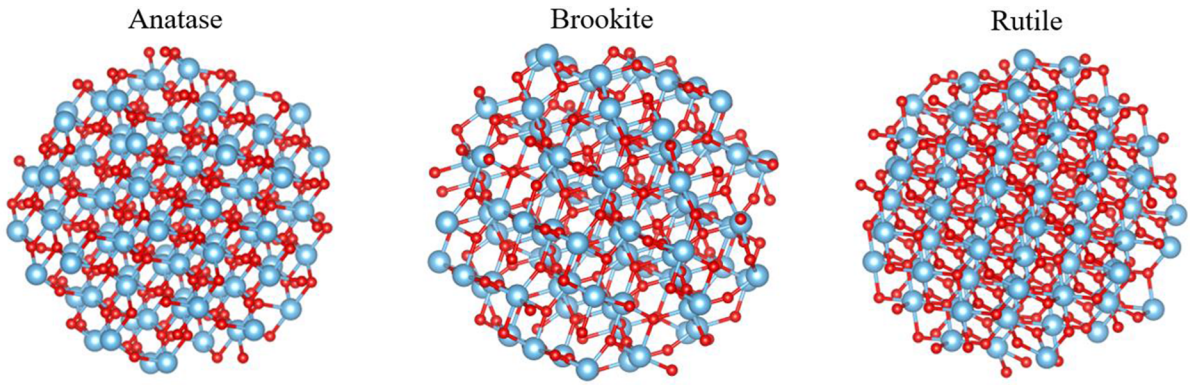

Fig. 1. Initial structures of the anatase, brookite and rutile phase TiO_2 nanoparticles (Ti is blue, O is red).

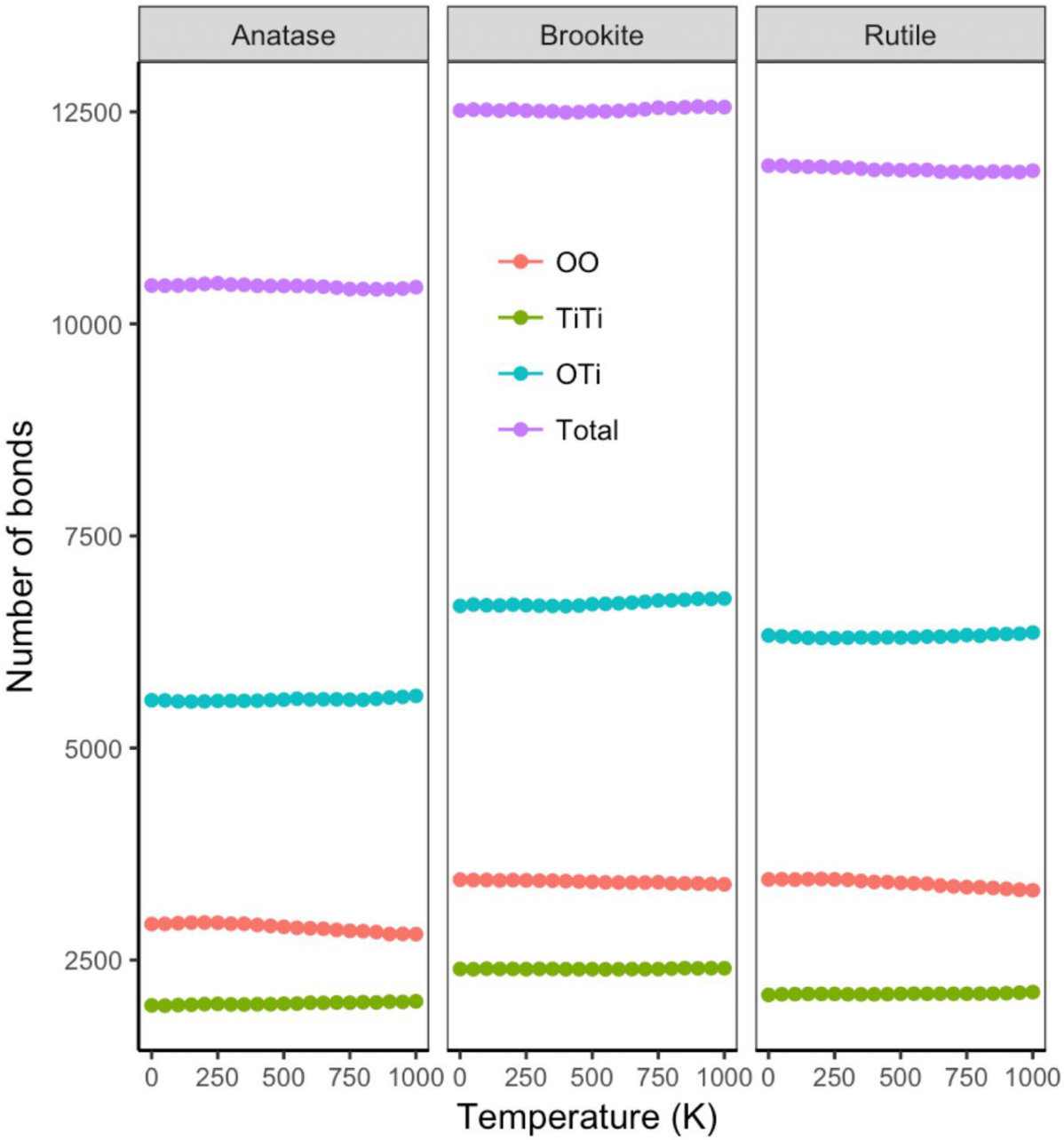

Fig. 2. Variation of number of bonds of binary O-O, Ti-Ti and O-Ti interactions as a function of temperature.

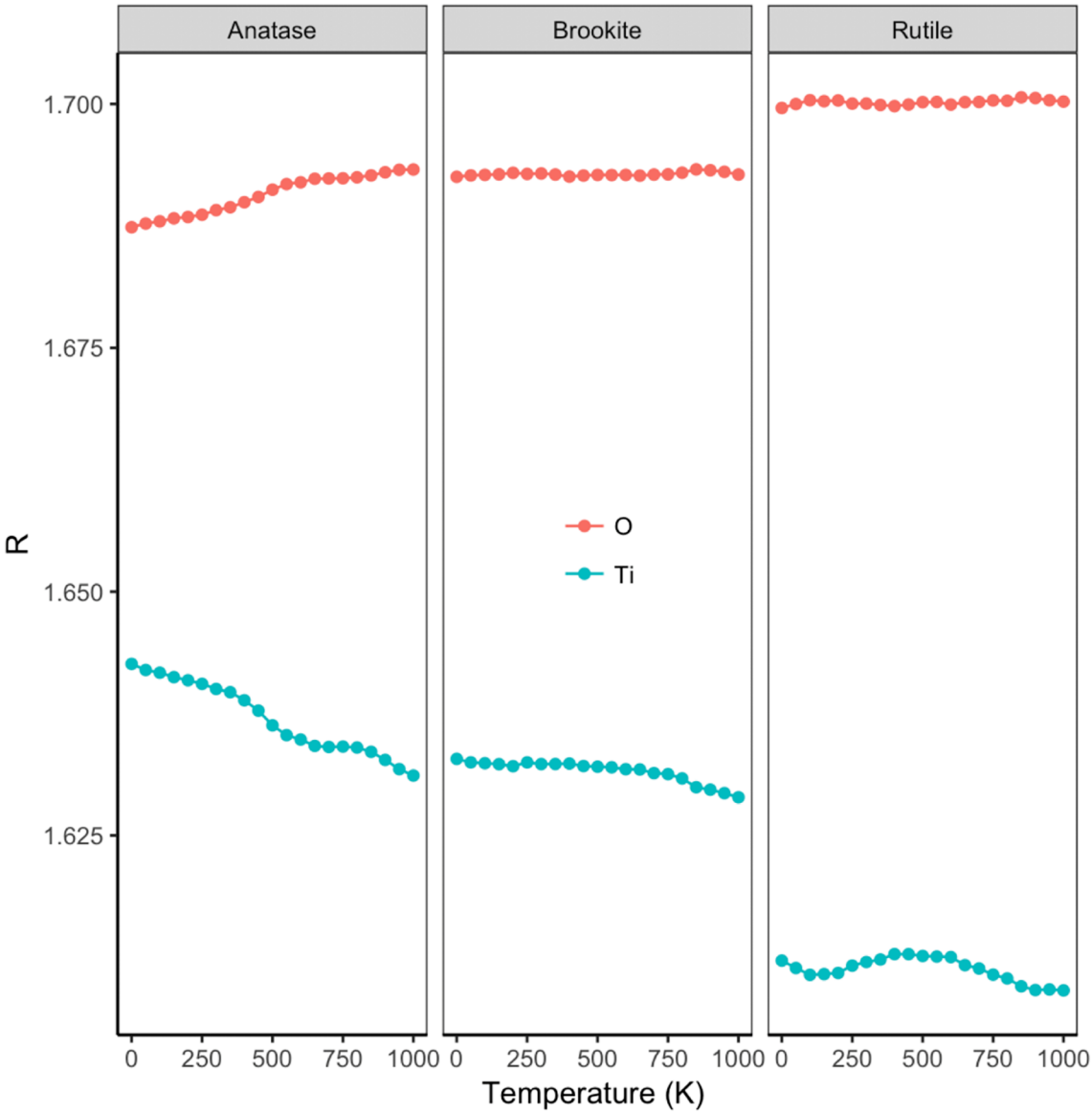

Fig. 3. Temperature dependence of the order parameter of O and Ti atoms in the anatase, brookite and rutile phase TiO_2 nanoparticles.

between Ti-Ti, Ti-O and O-O binary interactions in of anatase, brookite and rutile phase TiO_2 NPs. To conduct structural analysis, we have developed programs in the R language (discussed in the next section) to analyze the number of bonds, segregation phenomena, and RDF.

2. The method of calculations

The structural analysis and electronic structure of anatase, brookite and rutile phase TiO_2 NPs have been investigated using DFTB and molecular dynamics methods implemented in DFTB + code [38] with the hyb-0–2 [39,40] set of Slater Koster parameters. We do not explain the procedure for DFTB calculations here, since there currently exist several studies available with detailed descriptions of both theoretical aspects and performance of the DFTB approach, including advances in theoretical development and application [41–44]. The initial structures of anatase, brookite and rutile phase TiO_2 NPs are indicated in Fig. 1. All of three TiO_2 NP models were carved from a bulk 60 × 60 × 60 supercell. The radius of the NP is set to the desired value (0.9 nm), and only atoms within that sphere are considered, whereas those outside the sphere are removed. All calculations are performed at constant volume. To simplify the structural analysis, we have implemented programs in R—an open-source programming language that includes both an interactive environment and IDE-like versions—that is among the most ubiquitously used computational tools in data science. Our programs include functions to analyze the number of bonds, segregation phenomena, and RDF of anatase, brookite and rutile phase TiO_2 NPs. In our previous study, we obtained reasonable results based on our suite of programs [35]. We have made the code freely available online in GitHub. Additionally, these programs include high-resolution visualizations to plot data, though our intent is broader than the scope of the work in this paper in creating general, open-source tools for computational material science: (https://github.com/hasankurban/Structural-Analysis-NanoParticles).

3. Results and discussions

3.1. Structural analysis

The nearest neighbor contacts count,n_{ij}, (the number of bonds) is a significant property of NPs and used to differentiate the degree of packing in general. The number of bonds [45] for the NPs is given by

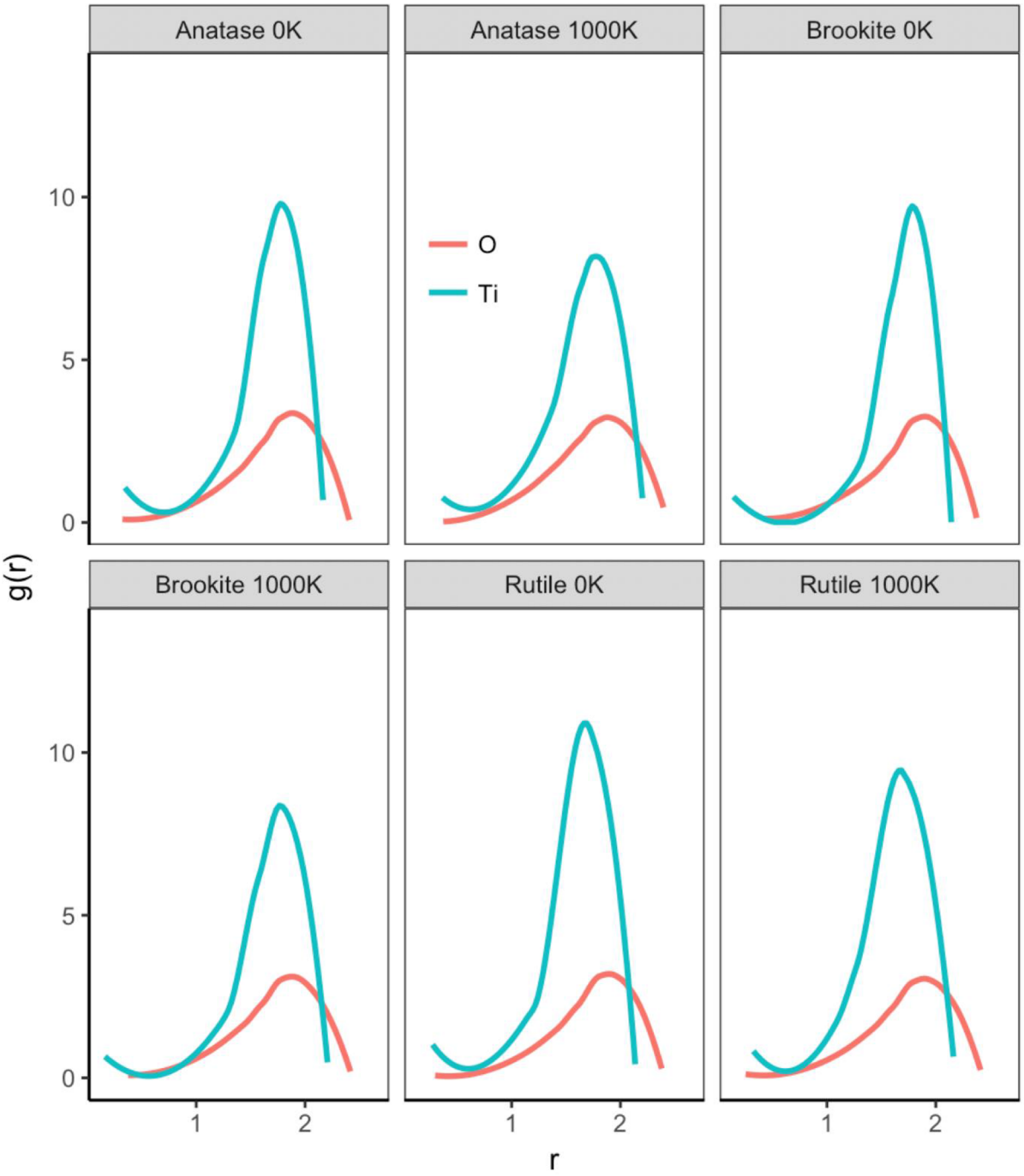

Fig. 4. Radial distribution function of the anatase, brookite and rutile phase TiO_2 nanoparticles at 0 K and 1000 K.

$$n_{ij} = \sum_{i<j} \delta_{ij} \tag{1}$$

where $\delta_{ij} = \begin{cases} 1, & r_{ij} \leq 1.2r_{ij}^{(0)} \\ 0, & r_{ij} > 1.2r_{ij}^{(0)} \end{cases}$ i, j= Ti or O, r_{ij} is the distance between atom i and j and $r_{ij}^{(0)}$ is a nearest neighbor criterion derived by fitting the experimental data [46]. In this study we investigate the atomic distribution of Ti and O atoms in the TiO_2 NPs using n_{ij}. Algorithms 1 (given as Supporting information), where D is the centered data set at the origin, denote the smallest distance between binary interactions (line 2), explains this process. The algorithm first calculates new r_{ij} values and then compares these new r_{ij} values with $r_{ij}^{(0)}$ input values (line 5). Finally, Algorithm 1 outputs the nearest number contact counts for each binary interaction.

Fig. 2 shows the numbers of bonds in the anatase, brookite and rutile TiO_2 NPs with 268, 295 and 287 atoms, respectively. From the curve of TiO_2 NPs shown in Fig. 2, observe that the number of Ti-Ti, Ti-O bonds increases gradually with an increase in temperature of three phase NPs, but O-O bonds decrease. Furthermore, the number of Ti-Ti bonds is relatively fewer than that of O-O. This means that O atoms tend to form more bonds with Ti atoms: that O-O tend to scatter on the surface can, thus, be inferred. Moreover, the number of Ti-O bonds is greater than that of Ti-O and O-O bonds; therefore, it appears that O atoms have a greater preference for Ti atoms than for O atoms with increasing temperature. When comparing the number of bonds of different phases Ti-O, Ti-O and O-O, bonding of the anatase phase is greater than either brookite or rutile phase. On the other hand, we built open-source R programs mentioned above, to calculate several

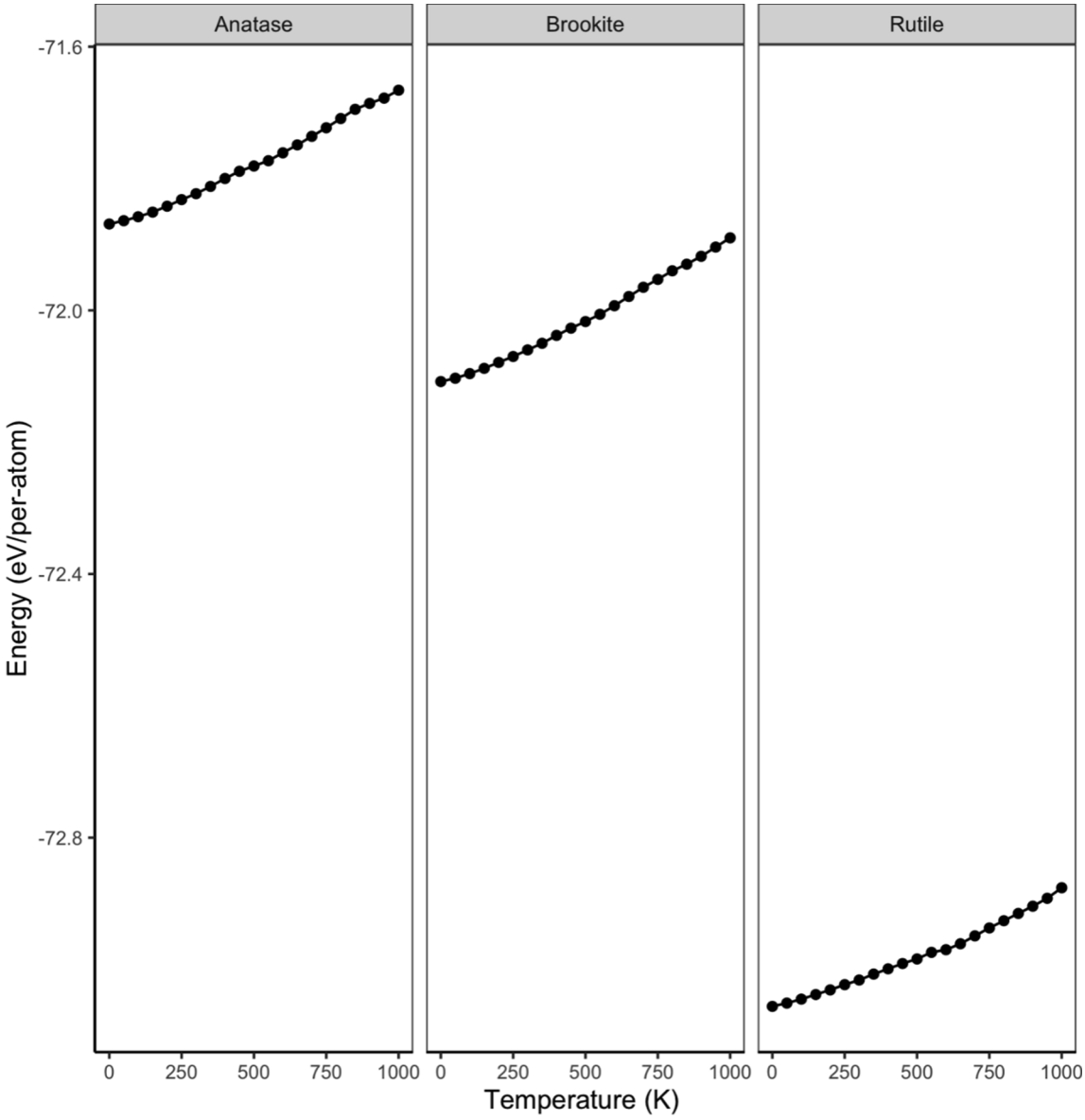

Fig. 5. Potential energy per/atom of the anatase, brookite and rutile phase TiO_2 nanoparticles as a function of temperature.

important metrics. To calculate the total number of bonds, our program separately finds the bond numbers between T-T, O-O and T-O interactions and then sum of them all.

One of the major problems of some materials [47] is the formation of a stable structure for obtaining high-efficiency devices. The distribution of atoms in crystalline structures is, in general, uniform and homogeneous [48]. In this context, in order to find the stable structure in NPs, we performed an in-depth analysis based on the order parameter (R_{T_i}) which analyzes the distribution of the different types of atoms [49]. Let n_{T_i}be the number T_i type atoms in the ternary ABCNPs, r_i the distance of the atoms to the coordinate center of the NP, then R_{T_i}, the average distance of a type T_i atoms in accordance with the center of a NP, is calculated as follows:

$$R_{T_i} = \frac{1}{n_{T_i}} \sum_{i=1}^{n_{T_i}} r_i \tag{2}$$

An $\in$ distance from center of NP to a reference point is defined to show the location of atoms; if $R_{T_i} < \epsilon_{min}$(a "small" value), it means that the T_i type atoms are at the center, and if $R_{T_i} > \epsilon_{max}$(a "large" value), it means that the T_i type atoms are at the surface region of NP. If neither is true, i.e., if $\epsilon_{min} \leq R_{T_i} \leq \epsilon_{max}$ (a "medium" value), it means a well-mixed NP. The R_{T_i} of each atom type is analyzed using Algorithm 2 given in Supporting information. The algorithm takes$D$, data set (Line 2), as an input and calculates the order parameter values R_{T_i} as shown in line 9 where n_{T_i}represents the number of atoms for atom type T_i and x_j, $y_j$and $z_j$are the coordinates of the atom j.

Fig. 3 shows the behavior of $R$of Ti and O atoms with temperature. The segregation behavior of atoms in the anatase, brookite and rutile phase TiO_2 NPs is determined using R. The segregation of Ti and O atoms under heat treatment shows that Ti atoms tend to locate at the center, while O atoms tend to occupy the surface as a general trend. The segregation of O atoms to the surface is due to its lower cohesive energy. The R value indicates different characteristics with increasing temperature of the TiO_2 NPs. $R_O$values of anatase phase TiO_2 NP sharply increase up to about 600 K and then smoothly increase while R_{Ti}decreases sharply for anatase phase NPs. On the other hand, $R_O$and R_{Ti}values of brookite and rutile phase TiO_2 NP slightly increase and decrease with temperature, respectively. It is interesting to note that there are some fluctuations have been observed for the R of rutile phase of TiO_2 NP—especially, Ti atoms which mainly tend to occupy the surface in the range of about 200 K to 500 K. The segregation of Ti

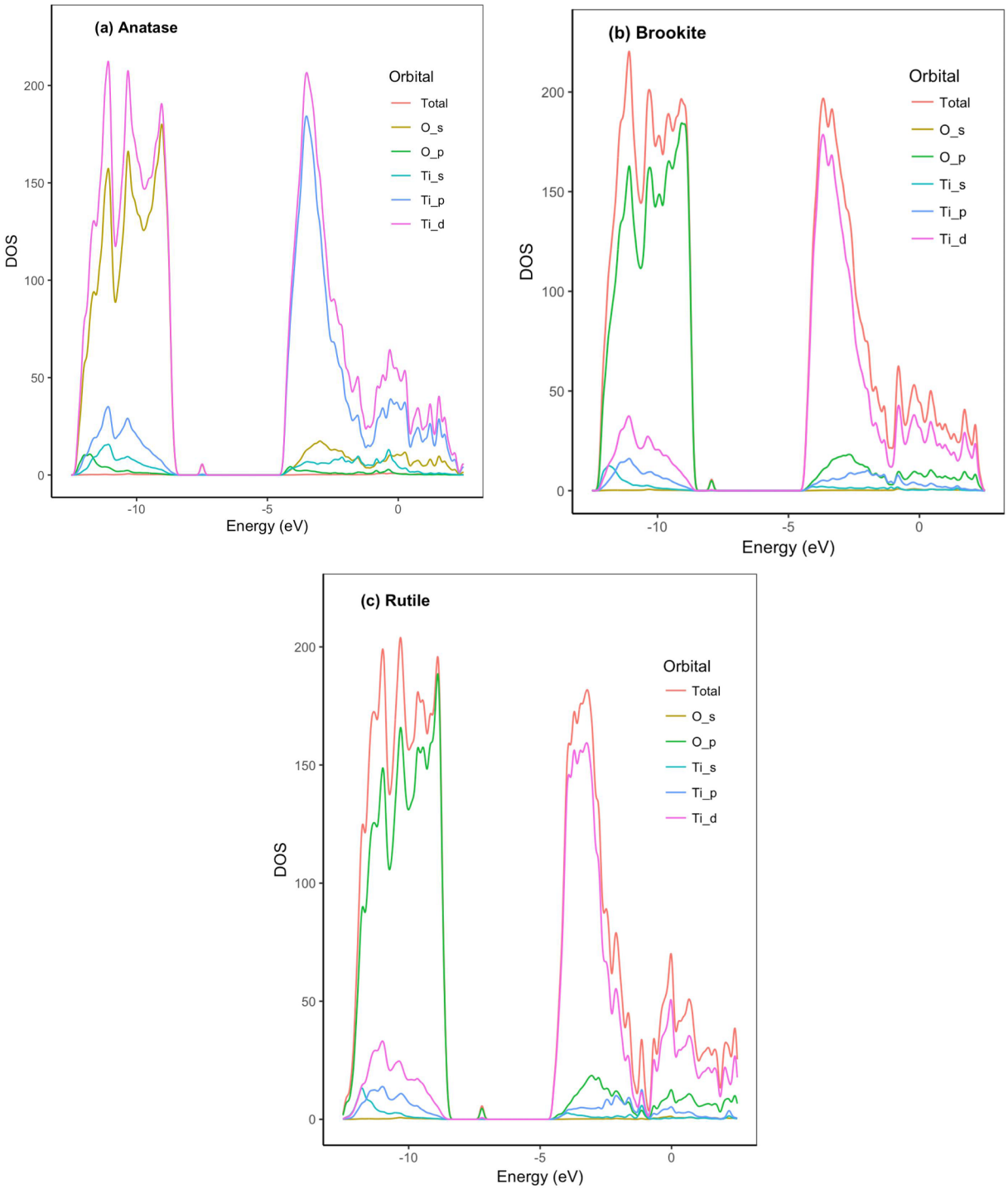

Fig. 6. The partial and total density of states (DOS) of the anatase, brookite and rutile phase TiO_2 nanoparticles.

atoms to the surface can be explained in terms of the lower surface energy and cohesive energy of Ti at about 200 K to 500 K.

Another substantial structural characteristic is the Radial Distribution Function (RDF) that estimates the likelihood of finding a particle at a distance *r* from another tagged particle. Algorithm 3 (given as Supporting information) explains the RDF over a data set D where the algorithm takes inputs D, a distance vector *r*, and a distance vector *dr* denoting the thickness of a spherical shell. Line 16 represents the definition of RDF where $n_{(ri)}$ is the mean number of atoms in a shell of width*dr* at distancer_i, |Δ| represents total atom number, $V_s$is the volume of the spherical shell, and V_d is the mean atom density.

Fig. 4 shows the RDF Ti-Ti and O-O binary interactions in the anatase, brookite and rutile phase TiO_2 NPs at 0 K and 1000 K to observe temperature effects. The RDFs are calculated for each atomic pair of optimized the TiO_2 NPs. Ti-Ti interactions have a narrower and higher distribution than O-O interactions. The broad peaks are observed in the range of 1–2 Å. With regard to temperature dependence, the maximum peak of rutile phase TiO_2 NP is greater than that of anatase and brookite phase NPs. As three phase TiO_2 NPs are heated from 0 K to 1000 K, the Ti and O atoms begin to oscillate about their equilibrium positions more rapidly, so the positions of the peaks change slightly because of a decrease in a well-defined obvious peaks in the RDF for Ti-

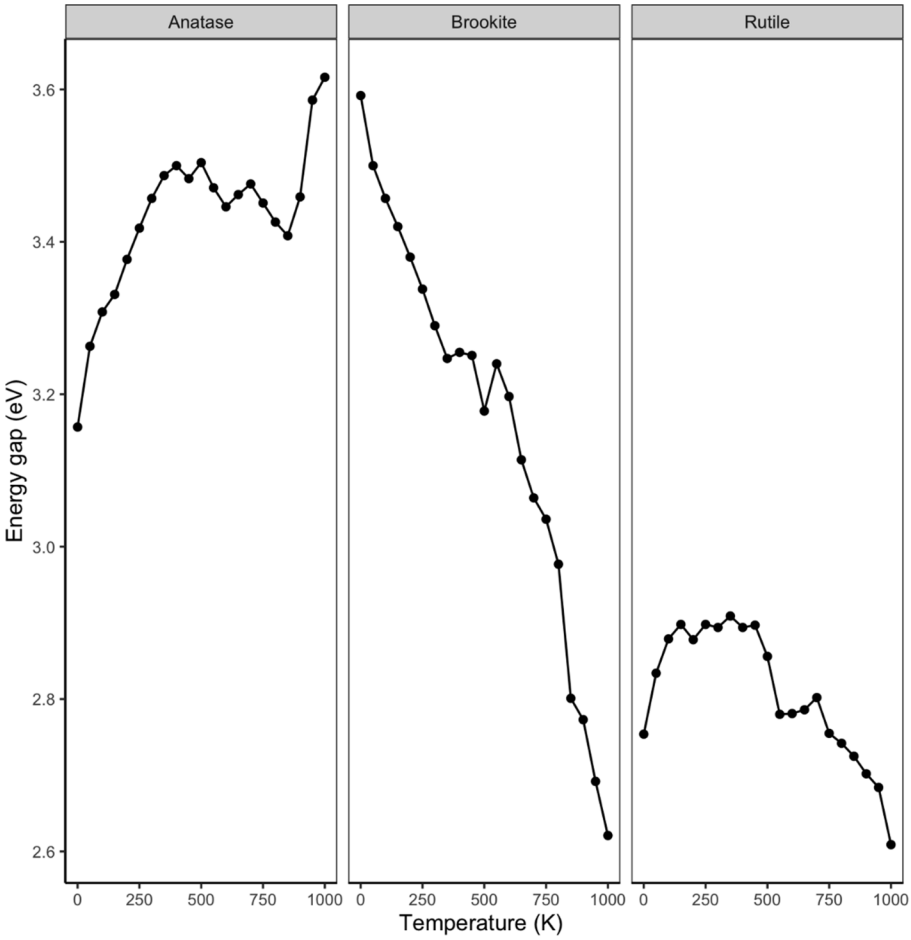

Fig. 7. The HOMO-LUMO energy gap of the anatase, brookite and rutile phase TiO_2 nanoparticles as a function of temperature.

Ti and O-O interactions. We point out that the calculated RDF peaks at radial distances between 1 and 2 Å in good agreement with experimental data [50].

Fig. 5 demonstrates the potential energy (E_p) per/atom, which is calculated by the subtraction of total energy from kinetic energy, of the anatase, brookite and rutile phase TiO_2 NPs as a function of temperature. In each case theE_p curve displays straight-line behavior in the range 100 K–1000 K. The $E_p$reflects the fact that anatase phase TiO_2 NP has the greater E_p than either brookite or rutile phase TiO_2 NPs due to both the difference of geometry and the number of atoms in the TiO_2 NPs.

3.2. Electronic structure

To obtain detailed information on electronic states in anatase, brookite and rutile phase TiO_2 NPs, we provide results of both the electronic partial and total DOS as shown in Fig. 6(a, b, and c). The density of localized states increases concomitantly with the temperature of TiO_2 NPs where the greatest contribution comes from the *d*-orbital of Ti atoms and *p*-orbital of O atoms. The fluctuations considerably change based upon the phase of TiO_2 NPs. In the valence band of O localized *p* states dominate, while in the conduction band of Ti localized *d* states dominate. The DOS analyses also indicate that anatase, brookite and rutile phase TiO_2 have bandgaps with values 3.15, 3.59 and 2.75 eV, respectively. According to experimental observations, TiO_2 NPs have the optical bandgap values of 3.21 eV for anatase, 3.13 eV for brookite, and 3.0 eV for rutile phases corresponding to indirect band gaps, and 3.53 eV for anatase, 3.56 eV for brookite and 3.37 eV for rutile phases corresponding to direct band gaps [14]. From the bandgap values obtained from measurements, we can conclude that the predicted bandgaps of anatase and rutile phase NPs have indirect transitions, but the brookite phase has direct transition. The predicted results in this study, therefore, are compatible and consistent with experimental data. The band gap variations were studied by interpreting the DRS data, and we observed that the bandgap of brookite and rutile phase TiO_2 NPs were reduced from 3.59 eV to 2.62 eV and from 2.75 eV to 2.60 eV, respectively because of the structural modifications with temperature in the NPs. Therefore, by reducing the bandgap of brookite and rutile TiO_2 NPs, the performance of energy storage and conversion devices can be enhanced [51–53]. On the other hand, the bandgap of anatase phase TiO_2 NP conversely increase from 3.15 eV to 3.61 eV. The bandgap of bulk anatase TiO_2 thin film, however, was reported to shift from around 3.15 eV at 300 K, 2.96 eV at 530 K [54]. In a recent experimental study, the bandgaps of anatase NP (12 nm) and rutile NP (49 nm) were measured to be 3.38 eV (at 723 K) and 3.03 eV (at 973 K), respectively [55], which are compatible with our results where the bandgap is calculated 3.45 eV (at 748 K) for anatase NP. We note that increasing temperatures resulted in fluctuations on the bandgap energy. For example, the bandgap of anatase phase TiO_2 NP increases from 3.15 eV at 0 K to 3.50 eV at 500 K, then, an increasing bandgap energy value was observed at temperature between 550 K and 850 K. After that, the bandgap increases from 900 K to 1000 K (see Fig. 7). These predicted changes and fluctuations under heat treatment in the bandgap energy for the different phases were also observed in the experimental study [56].

When it comes to the HOMO, LUMO and Fermi energy levels (see Fig. 8), there are a decrease and an increase in HOMO, LUMO, and Fermi energy with increasing temperature of anatase, brookite and

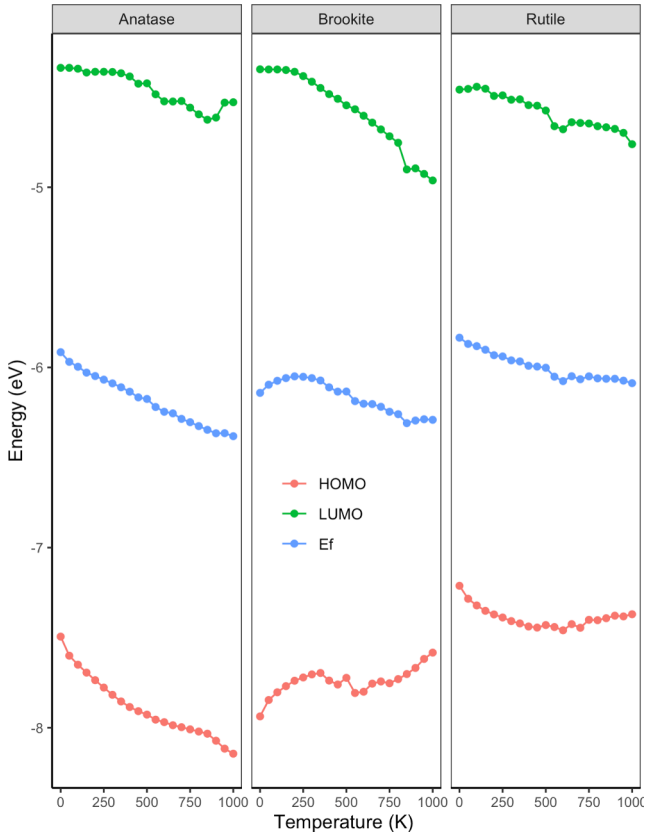

Fig. 8. HOMO, LUMO and Fermi energies of the anatase, brookite and rutile phase TiO_2 nanoparticles as a function of temperature.

rutile phase TiO_2 NPs. For three phase TiO_2 NPs, the LUMO and Fermi energy levels decrease with temperature. The HOMO value of anatase phase decreases, while it increases for brookite and rutile phases.

4. Conclusion

In this study, we have investigated the temperature dependence of structural and electronic properties of anatase, brookite and rutile phase TiO_2 NPs using the DFTB approach. To perform structural analysis, we designed, implemented, and tested R code which can be easily used by non-programmers to analyze the number of bonds, segregation phenomena, and RDFs of binary interactions in anatase, brookite and rutile phase TiO_2 NPs. From the results of our calculations, we found that the number of Ti-O bonds is larger than that of Ti-O and O-O bonds; therefore, it appears that O atoms have a greater preference for Ti atoms than for O atoms with temperature. The segregation of Ti and O atoms under heat treatment show that Ti atoms tend to locate at the center, while O atoms tend to occupy the surface as a general trend. The bandgap of brookite and rutile phase TiO_2 NPs are reduced from 3.59 eV to 2.62 eV and from 2.75 eV to 2.60 eV, respectively, which leads to visible light activity, and, thus, the performance of energy storage and conversion devices likely can be enhanced. The obtained electronic properties are found to be compatible with experimental findings.

CRediT authorship contribution statement

Hasan Kurban: Software, Visualization, Resources, Writing - review & editing. **Mehmet Dalkilic:** Writing - review & editing. **Selçuk Temiz:** Investigation. **Mustafa Kurban:** Supervision, Project administration, Investigation, Conceptualization, Writing - original draft, Writing - review & editing, Data curation, Validation, Software.

Declaration of Competing Interest

The authors declare that they have no known competing financial interests or personal relationships that could have appeared to influence the work reported in this paper.

Acknowledgments

The numerical calculations were also partially performed at TUBITAK ULAKBIM, High Performance and Grid Computing Centre (TRUBA resources), Turkey.

Data availability

The raw/processed data required to reproduce these findings cannot be shared at this time as the data also forms part of an ongoing study.

Appendix A. Supplementary data

Supplementary data to this article can be found online at https://doi.org/10.1016/j.commatsci.2020.109843.

References

[1] Akira Fujishima, Xintong Zhang, Donald A. Tryk, TiO_2 photocatalysis and related surface phenomena, Surf. Sci. Rep. 63 (12) (2008) 515–582.
[2] Samira Bagheri, Kamyar Shameli, Sharifah Bee Abd Hamid, Synthesis and characterization of anatase titanium dioxide nanoparticles using egg white solution via Sol-Gel method, J. Chem. 2012 (2013) 1–5.
[3] R. Palcheva, et al., TiO2 nanotubes supported NiW hydrodesulphurization catalysts: characterization and activity, Appl. Surf. Sci. 265 (2013) 309–316.
[4] Guanfeng Liang, et al., The hydrogenation/dehydrogenation activity of supported Ni catalysts and their effect on hexitols selectivity in hydrolytic hydrogenation of cellulose, J. Catal. 309 (2014) 468–476.
[5] Qiquan Luo, Matthias Beller, Haijun Jiao, Formic acid dehydrogenation on surfaces—a review of computational aspect, J. Theor. Comput. Chem. 12 (07) (2013) 1330001.
[6] Hiroshi Kominami, et al., Novel synthesis of microcrystalline titanium (IV) oxide having high thermal stability and ultra-high photocatalytic activity: thermal decomposition of titanium (IV) alkoxide in organic solvents, Catal. Lett. 46 (3-4) (1997) 235–240.
[7] Murray, C. Bea, David J. Norris, Moungi, G. Bawendi, Synthesis and characterization of nearly monodisperse CdE (E= sulfur, selenium, tellurium) semiconductor nanocrystallites, J. Am. Chem. Soc. 115 (19) (1993) 8706–8715.
[8] Tim Luttrell, et al., Why is anatase a better photocatalyst than rutile?-Model studies on epitaxial TiO 2 films, Sci. Rep. 4 (1) (2014) 1–8.
[9] G. Sivalingam, et al., Photocatalytic degradation of various dyes by combustion synthesized nano anatase TiO_2, Appl. Catal. B 45 (1) (2003) 23–38.
[10] Rajini P. Antony, et al., Efficient photocatalytic hydrogen generation by Pt modified TiO2 nanotubes fabricated by rapid breakdown anodization, Int. J. Hydrogen Energy 37 (10) (2012) 8268–8276.
[11] Marta Buchalska, et al., On oxygen activation at rutile-and anatase-TiO_2, ACS Catal. 5 (12) (2015) 7424–7431.
[12] Xiaobo Chen, Samuel S. Mao, Titanium dioxide nanomaterials: synthesis, properties, modifications, and applications, Chem. Rev. 107 (7) (2007) 2891–2959.
[13] Huang-Lin Kuo, et al., A highly active bi-crystalline photocatalyst consisting of TiO_2 (B) nanotube and anatase particle for producing H_2 gas from neat ethanol, Catal. Lett. 113 (1-2) (2007) 7–12.
[14] David Reyes-Coronado, et al., Phase-pure TiO_2 nanoparticles: anatase, brookite and rutile, Nanotechnology 19 (14) (2008) 145605.
[15] Gang Liu, et al., Synergistic effects of B/N doping on the visible-light photocatalytic activity of mesoporous TiO_2, Angew. Chem. Int. Ed. 47 (24) (2008) 4516–4520.
[16] Kantam, M. Lakshmi, et al., Synthesis of 2-indolyl-1-nitroalkane derivatives using nanocrystalline titanium (IV) oxide, Synthetic Commun. 39 (22) (2009) 4100–4108.
[17] Mohammad Rahimizadeh, et al., TiO_2 nanoparticles: an efficient heterogeneous catalyst for synthesis of bis (indolyl) methanes under solvent-free conditions, Monatshefte für Chemie-Chemical Monthly 140 (12) (2009) 1465–1469.
[18] Mirjalili, Bi Bi Fatemeh, Ali Akbari, Nano-TiO_2: an Eco-friendly and Re-usable Catalyst for the One-pot Synthesis of β-Acetamido Ketones, Zeitschrift für Naturforschung B 64 (3) (2009) 347–350.
[19] Mahmoud Nasrollahzadeh, et al., Preparation, optical properties and catalytic activity of TiO2@ Pd nanoparticles as heterogeneous and reusable catalysts for ligand-free Heck coupling reaction, J. Mol. Catal. A: Chem. 394 (2014) 205–210.
[20] B. Sreedhar, Divya Yada, P. Surendra Reddy, Nanocrystalline Titania-Supported Palladium (0) Nanoparticles for Suzuki-Miyaura Cross-Coupling of Aryl and Heteroaryl Halides, Adv. Synth. Catal. 353 (14-15) (2011) 2823–2836.
[21] Mahmoud Nasrollahzadeh, S. Mohammad Sajadi, Green synthesis, characterization

and catalytic activity of the Pd/TiO_2 nanoparticles for the ligand-free Suzuki-Miyaura coupling reaction, J. Colloid Interface Sci. 465 (2016) 121–127.
[22] Michele Melchionna, et al., Highly efficient hydrogen production through ethanol photoreforming by a carbon nanocone/Pd@ TiO_2 hybrid catalyst, Chem. Commun. 52 (4) (2016) 764–767.
[23] Mahmood Tajbakhsh, et al., Titanium dioxide nanoparticles catalyzed synthesis of Hantzsch esters and polyhydroquinoline derivatives, Chin. J. Catal. 33 (9-10) (2012) 1517–1522.
[24] Ali Khalafi-Nezhad, et al., An efficient one-pot access to quinazolinone derivatives using TiO_2 nanoparticles as catalyst: synthesis and vasorelaxant activity evaluation, Synlett 23 (06) (2012) 920–924.
[25] Mona Hosseini-Sarvari, Nano-tube TiO_2 as a new catalyst for eco-friendly synthesis of imines in sunlight, Chin. Chem. Lett. 22 (5) (2011) 547–550.
[26] Mirjalili, Bi Bi Fatemeh, Ali Akbari, Nano-TiO_2: an eco-friendly alternative for the synthesis of quinoxalines, Chin. Chem. Lett. 22 (6) (2011) 753–756.
[27] Th. Maggos, et al., Photocatalytic degradation of NOx in a pilot street canyon configuration using TiO_2-mortar panels, Environ. Monit. Assess. 136 (1-3) (2008) 35–44.
[28] Michael R. Hoffmann, et al., Environmental applications of semiconductor photocatalysis, Chem. Rev. 95 (1) (1995) 69–96.
[29] Tijana Rajh, et al., Titanium dioxide in the service of the biomedical revolution, Chem. Rev. 114 (19) (2014) 10177–10216.
[30] Rajh, Tijana, NadaM. Dimitrijevic, Elena A. Rozhkova, Titanium dioxide nanoparticles in advanced imaging and nanotherapeutics, Biomedical Nanotechnology, Humana Press, 2011, pp. 63–75.
[31] Alvarez Barragan, Niranjan V. Alejandro, Lanlan Zhong Ilawe, Bryan M. Wong, Lorenzo Mangolini, A non-thermal plasma route to plasmonic TiN nanoparticles, J. Phys. Chem. C 121 (4) (2017) 2316–2322.
[32] Mustafa Kurban, Electronic structure, optical and structural properties of Si, Ni, B and N-doped a carbon nanotube: DFT study, Optik 172 (2018) 295–301.
[33] Mustafa Kurban, Tunable electronic structure and structural transition of GaAs clusters at high pressure and temperature, J. Alloy. Compd. 791 (2019) 1159–1166.
[34] Mustafa Kurban, Hasan Kurban, Study of Structural and Optoelectronic Properties of Hexagonal ZnO Nanoparticles, Bilecik Şeyh Edebali Univ. J. Sci. 6 (2) (2019) 124–131.
[35] Hasan Kurban, Mustafa Kurban, Mehmet Dalkılıç, Density-functional tight-binding approach for the structural analysis and electronic structure of copper hydride metallic nanoparticles, Mater. Today Commun. 21 (2019) 100648.
[36] Niranjan V. Ilawe, M. Belén Oviedo, Bryan M. Wong, Effect of quantum tunneling on the efficiency of excitation energy transfer in plasmonic nanoparticle chain waveguides, J. Mater. Chem. C 6 (22) (2018) 5857–5864.
[37] Niranjan V. Ilawe, M. Belén Oviedo, Bryan M. Wong, Real-time quantum dynamics of long-range electronic excitation transfer in plasmonic nanoantennas, J. Chem. Theory Comput. 13 (8) (2017) 3442–3454.
[38] Balint Aradi, Ben Hourahine, Th. Frauenheim, DFTB+, a sparse matrix-based implementation of the DFTB method, J. Phys. Chem. A 111 (26) (2007) 5678–5684.
[39] Regina Luschtinetz, et al., Adsorption of phosphonic acid at the TiO2 anatase (101) and rutile (110) surfaces, J. Phys. Chem. C 113 (14) (2009) 5730–5740.
[40] Sibylle Gemming, et al., Adsorption of nucleotides on the rutile (110) surface, Int. J. Mater. Res. 101 (6) (2010) 758–764.
[41] Shahidul M. Islam, Pierre-Nicholas Roy, Performance of the SCC-DFTB model for description of five-membered ring carbohydrate conformations: comparison to force fields, high-level electronic structure methods, and experiment, J. Chem. Theory Comput. 8 (7) (2012) 2412–2423.
[42] Matthew A. Addicoat, et al., Assessment of the density functional tight binding method for protic ionic liquids, J. Chem. Theory Comput. 10 (10) (2014) 4633–4643.
[43] Th. Frauenheim, et al., A self-consistent charge density-functional based tight-binding method for predictive materials simulations in physics, chemistry and biology, Phys. Status Solidi (b) 217 (1) (2000) 41–62.
[44] Thomas Frauenheim, et al., Atomistic simulations of complex materials: ground-state and excited-state properties, J. Phys.: Condens. Matter 14 (11) (2002) 3015.
[45] Xia Wu, et al., Structure and bonding in quaternary AgAuPdPt clusters, J. Alloy. Compd. 687 (2016) 115–120.
[46] P. Kania, et al., Millimeter-wave spectroscopy of titanium dioxide, TiO_2, J. Mol. Spectrosc. 268 (1-2) (2011) 173–176.
[47] T.-C. Yu, R.F. Brebrick, The Hg-Cd-Zn-Te Phase Diagram, Journal of Phase Equilibria 13 (5) (1992) 476–496.
[48] Chenxi Lu, et al., One-dimensional growth of zinc crystals on a liquid surface, Sci. Rep. 6 (1) (2016) 1–7.
[49] Mustafa Kurban, O. Barış Malcıoğlu, Şakir Erkoç, Structural and thermal properties of Cd–Zn–Te ternary nanoparticles: Molecular-dynamics simulations, Chem. Phys. 464 (2016) 40–45.
[50] Hengzhong Zhang, et al., Atomic structure of nanometer-sized amorphous TiO_2, Phys. Rev. B 78 (21) (2008) 214106.
[51] Wei Xie, Rui Li, Xu. Qingyu, Enhanced photocatalytic activity of Se-doped TiO_2 under visible light irradiation, Sci. Rep. 8 (1) (2018) 1–10.
[52] Christian Dette, et al., TiO2 anatase with a bandgap in the visible region, Nano Lett. 14 (11) (2014) 6533–6538.
[53] Mohammad Ehtisham Khan, et al., Microbial fuel cell assisted band gap narrowed TiO_2 for visible light-induced photocatalytic activities and power generation, Sci. Rep. 8 (1) (2018) 1–12.
[54] Fan Zhang, et al., Temperature-dependent optical properties of titanium oxide thin films studied by spectroscopic ellipsometry, Appl. Phys. Express 6 (12) (2013) 121101.
[55] R.S. Dubey, Temperature-dependent phase transformation of TiO2 nanoparticles synthesized by sol-gel method, Mater. Lett. 215 (2018) 312–317.
[56] Tao Peng, et al., The role of hydrothermal conditions in determining 1D TiO_2 nanomaterials bandgap energies and crystal phases, Mater. Res. Bull. 105 (2018) 104–113.